CD Stretching Modes are Sensitive to the Microenvironment in Ionic Liquids

Thorben Sieling,[a] Thorben Petersen,[a] Torben Alpers,[a] Jens Christoffers,[a] Thorsten Klüner,[a] and Izabella Brand*[a]

Abstract: Knowledge of the structure of the electrical double layer in ionic liquids (IL) is crucial for their applications in electrochemical technologies. We report the synthesis and applicability of an imidazolium-based amphiphilic ionic liquid with a perdeuterated alkyl chain for studies of electric potential-dependent rearrangements, and changes in the microenvironment in a monolayer on a Au(111) surface. Electrochemical measurements show two states of the organization of ions on the electrode surface. In situ IR spectroscopy shows that the alkyl chains in imidazolium cations change their orientation depending on the adsorption state. The methylene-d_2 stretching modes in the perdeuterated IL display a reversible, potential-dependent appearance of a new band. The presence of this mode also depends on the anion in the IL. Supported by quantum chemical calculations, this new mode is assigned to a second $\nu_{as}(CD_2)$ band in alkyl-chain fragments embedded in a polar environment of the anions/solvent present in the vicinity of the imidazolium cation and electrode. It is a measure of the potential-dependent segregation between polar and nonpolar environments in the layers of an IL closest to the electrode.

Introduction

Ionic liquids (ILs) are usually composed of bulky organic cations and either organic or inorganic anions. Large size and asymmetric charge distribution destabilize the crystal lattice of the salt and result in low melting temperatures of ILs. They find applications in catalysis, electrocatalysis, electrostatic catalysis, double layer capacitors, batteries, liquids for electroplating, membranes for the capture of gases (for example, CO_2), solvents facilitating biodegradation processes, and even antibacterial drugs.[1] Their diverse applications resulted in a huge structural diversity of the available ILs. The ions of ILs, in particular cations, contain polar and nonpolar moieties. The introduction of an alkyl chain may grant an amphiphilic character to an ion of ILs. Based on this criterion, two classes of ILs have been defined: non-amphiphilic ionic liquids and amphiphilic, surface-active ionic liquids.[1a,b,2] The asymmetric structure of ions results in both electrostatic interactions between charged, polar residues and dispersive van der Waals interactions between nonpolar residues. In the bulk phase, the polar and nonpolar residues segregate into nanoaggregated structures.[3] In ILs, the nonpolar fragment of an ion occupies a larger volume than the charged moiety, resulting in formation of various self-assembled structures.[1a,4]

Exposure of ILs to a phase boundary (IL | gas or IL | solid) introduces another level into the complexity of structural features formed by ILs, in particular by amphiphilic ILs.[2a,3a,5] In general, ILs at interfaces adopt a multilayer structure composed of alternating layers of cations and anions.[2a,3a,5a,b,6] The composition, structure, and thickness of these ordered multilayers depend on the surface charge density of the solid substrate. The use of electrodes allows for controlling the electric potentials, and leads to dynamic, potential-dependent changes in the composition and structure of the electrical double layer of ILs. ILs have relatively slow reorganization dynamics of their electrical double layer, as proven by the appearance of a hysteresis in electrochemical measurements and simulations.[4a,5b,7] There is clear experimental evidence that in some ILs (for example, 1-methyl-3-(dodecyl)imidazolium bis (trifluoromethylsulfonyl)imide), or 1-hexyl-3-(methyl) imidazolium chloride) the multilayer structure of the electrical double layer is disrupted by the formation of three-dimensional aggregates[6c,8] The molecular-scale order in the nanostructures of ILs changes as a function of the applied electric potentials, or upon the controlled addition of solvents. These two factors contribute to the structure and capacitance of the electrical double layer of ILs, and therefore may affect the progress of electrochemical reactions occurring in ILs and their mixtures.[1b,2a] Thus, recognition of the potential-dependent changes in the composition, size, molecular-scale organization, and structure of nanoaggregates of ions in ILs present in the layers closest to the electrode is of great scientific interest and importance.

[a] T. Sieling, Dr. T. Petersen, Dr. T. Alpers, Prof. Dr. J. Christoffers, Prof. Dr. T. Klüner, Dr. I. Brand
Institute of Chemistry
University of Oldenburg
26111 Oldenburg (Germany)
E-mail: Izabella.brand@uni-oldenburg.de

Supporting information for this article is available on the WWW under https://doi.org/10.1002/chem.202102346

Distinguishing the layers of an IL closest to the electrode from its bulk phase remains a significant experimental challenge. Infrared spectroscopy (IRS) techniques are extremely useful for in situ studies of the composition, structure, conformation, and orientation of organic molecules in their assemblies at electrode surfaces.[9] A great advantage of IRS arises from the ability to simultaneously identify the composition and structure of different components in a complex molecular assembly, because various functional groups absorb IR light at distinct wavenumbers. In addition, an IR spectrum is sensitive to the sample environment. Methyl and methylene groups are present in numerous ions of ILs. In a saturated alkyl chain, these groups give rise to symmetric and asymmetric stretching modes in the 2970–2840 cm^{-1} spectral region. These fundamental modes overlap with overtones and binary combination of CH deformation modes enhanced by Fermi resonance,[10] hampering the analysis of the conformation, packing, and aggregation state of alkyl chains in molecular assemblies such as the electrical double layer of ILs.[11] This can be ameliorated through a substitution of the hydrogen atoms by deuterium. Isotopic substitution of H by D leads to a ca. 700 cm^{-1} bathochromic shift of the corresponding methyl and methylene stretching modes. The 2200–2000 cm^{-1} spectral region does not interfere with IR absorption modes of other functional groups, allowing for an in-depth analysis of the effect of the local environment on the position and intensities of the methylene-d_2 and methyl-d_3 stretching modes.[12] Conveniently, substitution of H atoms by D perturbs the chemical and physical properties of the alkyl-chain fragment of a target molecule to a small extent.

ILs with perdeuterated alkyl chains are very rare[13] and, to the best of our knowledge, their use for the description of structural changes occurring in the electrical double layer of ILs has not previously been explored. In this work, we describe the synthesis of an amphiphilic IL with a perdeuterated alkyl chain. Furthermore, we used the perdeuterated [C18C1Im-d_{37}][TfO] to prepare a Langmuir-Blodgett (LB) monolayer on the Au(111) electrode surface. In the monolayer film the imidazolium ring makes a direct contact to the Au surface whereas the perdeuterated octadecyl chain is ordered toward the electrolyte solution.[11a] Counterions from the subphase (ClO_4^- or Cl^-) ions are transferred onto the Au(111) surface. Based on our previous XPS results, some anions make a direct contact to the Au(111) surface while others are present in the film.[11a,14] The exact position of the anions is unknown but assumed to change flexibly. This monolayer film served as the electrode-closest model of the electrical double layer of ILs. The response of the IL monolayer to electric potentials was investigated using electrochemistry and in situ polarization modulation infrared reflection absorption spectroscopy (PM IRRAS). In the monolayers, in contrast to a bulk phase, the IR spectrum of the [C18C1Im-d_{37}][TfO] IL showed a new IR absorption band centered at 2183 cm^{-1}. The appearance of this mode and its intensity depended on the potential applied to the electrode and the chemical nature of the anion present in the solution. To understand the nature of this new mode, quantum chemical calculations were conducted. Based on the experimental and computed IR spectra, we assigned this new absorption band to a second $\nu_{as}(CD_2)$ band. A simultaneous potential-driven movement of anions and rearrangement of alkyl chains in the cations change the composition of the electrical double layer. These rearrangements are responsible for local changes between polar and nonpolar environment, a driving force for the nanosegregation process in the monolayer.

Results and Discussion

Synthesis of [C18C1Im-d_{37}][TfO]

The title compound of this study 1-methyl-3-(octadecyl) imidazolium trifluoromethanesulfonate was prepared in two steps from perdeuterated octadecanol, which was commercially available. First of all, the trifluoromethanesulfonic ester was prepared by conversion of the alcohol with the respective anhydride Tf_2O following a standard protocol.[15] The ester was then converted with *N*-methylimidazole at 130 °C in acetone (Scheme 1). The crude material was purified by recrystallization from *tert*-butylmethylether (MTBE, yield 72% of a colorless solid).

IR spectra of the [C18C1Im-d_{37}]$^+$-based ionic liquid

In the newly synthesized IL [C18C1Im-d_{37}][TfO], the cation has an amphiphilic character and forms stable, well-organized monolayers at the aqueous electrolyte (0.1 M $KClO_4$) | air interface. A vertical Langmuir-Blodgett (LB) deposition was used to fabricate a monolayer of the amphiphilic cation [C18C1Im-d_{37}]$^+$ on a Au(111) surface.[11a] During the formation of the monolayer at the electrolyte | air interface, the anion exchange took place.[11a,14] Our previous XPS studies showed that, together with the [C18C1Im-h_{43}]$^+$ cations, the ClO_4^- anions from the subphase were transferred onto the gold surface. Note that compound [C18C1Im-h_{43}][X] has exactly the same structure as [C18C1Im-d_{37}][X]. Both cations have *n*-octadecyl alkyl chains. The differ-

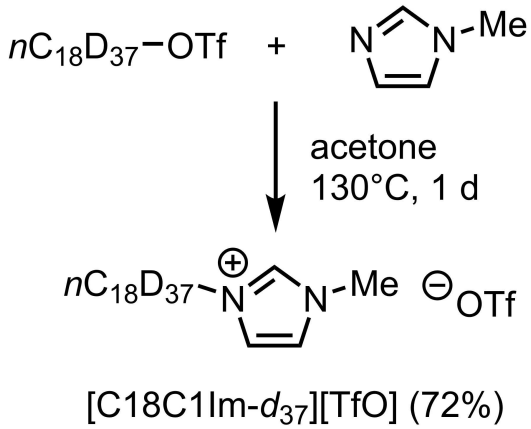

Scheme 1. Preparation of the 1-methyl-3-(octadecyl)imidazolium trifluoromethanesulfonate, [C18C1Im-d_{37}][TfO] IL.

ence of 5 H atoms, as written in the abbreviation of the cation, arises from the presence of H atoms in the imidazolium ring. Therefore, we use the abbreviation [C18C1Im-d_{37}][X] for the LB monolayer of the IL.

To understand the molecular level structure of the LB monolayer, IR spectra of the [C18C1Im-d_{37}] [TfO] IL and of the LB monolayers on the Au surface were measured. IR spectra in the CD stretching modes region of the [C18C1Im-d_{37}] [TfO] IL and LB films of the [C18C1Im-d_{37}][X] IL on the Au(111) surface are shown in Figure 1.

The ATR IR spectrum of the [C18C1Im-d_{37}][TfO] IL exhibited two intense IR absorption modes at 2195 and 2090 cm^{-1}, which are assigned to the $\nu_{as}(CD_2)$ and $\nu_s(CD_2)$ vibrations, respectively (Figure 1a). The full width at half maximum (fwhm) of each mode was extracted by deconvolution and fitting of the experimental spectra (S1, Supporting Information). The fwhm of the $\nu_{as}(CD_2)$ equaled 14 cm^{-1} and 10 cm^{-1} for the $\nu_s(CD_2)$ mode. The $\nu_{as}(CD_3)$ and $\nu_s(CD_3)$ modes in the terminal methyl group were located at 2215 and 2071 cm^{-1}, respectively. In the spectral range between 2100 and 2175 cm^{-1}, weak absorption bands appear in the IR spectra of perdeuterated alkanes.[12b,16] In the IR spectrum of the [C18C1Im-d_{37}][TfO] IL, the mode 2158 cm^{-1} was assigned to the first overtone of the CD_2 bending mode, being in Fermi resonance (FR) mode with the fundamental $\nu_s(CD_2)$ mode.[16d,17] Other weak modes in this spectral region arose from combination modes involving CD_3 deformation modes and combination modes of the $\delta(CD_2)$, ν(CC) modes.[18]

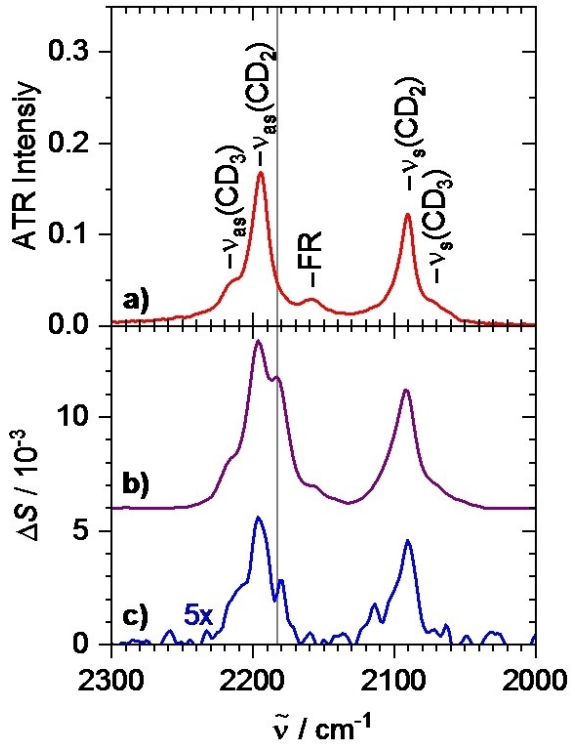

Figure 1. a) ATR spectrum of [C18C1Im-d_{37}][TfO] powder and b, c) PM IRRA spectra of the [C18C1Im-d_{37}][X] LB monolayer at the Au(111)|air interface transferred from aqueous 0.1 M $KClO_4$, b) single component and c) a two component [C18C1Im-d_{37}][X]:[C18C1Im-h_{43}][X] (1:10 molar ratio) LB monolayer. A thin solid line shows the position of the new IR absorption band.

In the PM IRRA spectra of the [C18C1Im-d_{37}][X] monolayers, all the described fundamental and FR modes were present (Figure 1b). The $\nu_{as}(CD_2)$ mode was centered at 2197 cm^{-1} and the $\nu_s(CD_2)$ at 2093 cm^{-1}. The fwhm of the $\nu_{as}(CD_2)$ mode equaled 15 cm^{-1} and 12 cm^{-1} for the $\nu_s(CD_2)$ mode (S1, Supporting Information). Compared to the ATR spectrum, they were shifted to higher wavenumbers and their fwhm were larger. This spectral characteristic allows for the elucidation of the physical state (conformation) of the alkyl chains in the [C18C1Im-d_{37}][X] monolayer film.[12a,16b,19] In the [C18C1Im-d_{37}][X] monolayer on the Au(111) surface, the positions of the methylene-d_2 stretching modes are characteristic for a liquid state of the perdeuterated alkane chains in the cation. The presence of a new IR absorption mode at 2182 cm^{-1} was specific to the [C18C1Im-d_{37}][X] monolayer deposited on the Au(111) surface (Figure 1b–c). The fwhm of this new band equaled 15 cm^{-1}. Assignment of this mode was not clear and is discussed below. Since IRS is sensitive to a long- and short-range molecular-scale order, and thus to inter- and intrachain interactions, isotopic dilution experiments were performed. Figure 1(c) shows a PMIRRA spectrum of a LB monolayer containing [C18C1Im-d_{37}][X]:[C18C1Im-h_{43}][X] in 1:10 molar ratio. Note, that both components of the monolayer have the same structure, one of them contains a perdeuterated [C18C1Im-d_{37}] while the second hydrogenated [C18C1Im-h_{43}] octadecyl chain. Since the spectrum in the isotopically diluted compound in the 2300–2000 cm^{-1} spectral region is very weak, the raw, background uncorrected spectra are shown for comparison in Figure S2 (Supporting Information). The isotopic dilution, besides for a decrease in intensity, resulted in no spectral changes of the analyzed above IR absorption modes and indicates that long-range interchain interactions are not responsible for the appearance of the new absorption mode. Thus, this new spectral feature was associated with the structure and environment of the IL film.

To understand the nature of the new IR absorption band, in situ experiments were performed. In these experiments, the [C18C1Im-d_{37}][X] monolayer was exposed to an aqueous electrolyte solution and changing electric potentials. Figure S3 (Supporting Information) shows the capacitance of the [C18C1Im-h_{43}][X] monolayer as a function of the electrode potential. Our previous studies showed that the structure of the [C18C1Im-h_{43}][X] monolayer depends on the potential applied to the Au(111) electrode.[11a] Briefly, the [C18C1Im-h_{43}][X] monolayer has two adsorption states: One occurs in the region of the capacitance minimum (5–7 μF cm^{-2}) (Figure S3, Supporting Information). A negative potential shift leads to a phase transition, and formation of the second adsorption state of the monolayer (capacitance 12–15 μF cm^{-2}). To follow electric potential-dependent changes in the composition and orientation of the cation in the IL film, in situ PM IRRA spectra of the [C18C1Im-d_{37}][X] monolayer were measured. Figure 2 shows large spectral changes as a function of the electrode potential. The CD stretching modes were well resolved from the background spectrum in both the positive- and negative-going

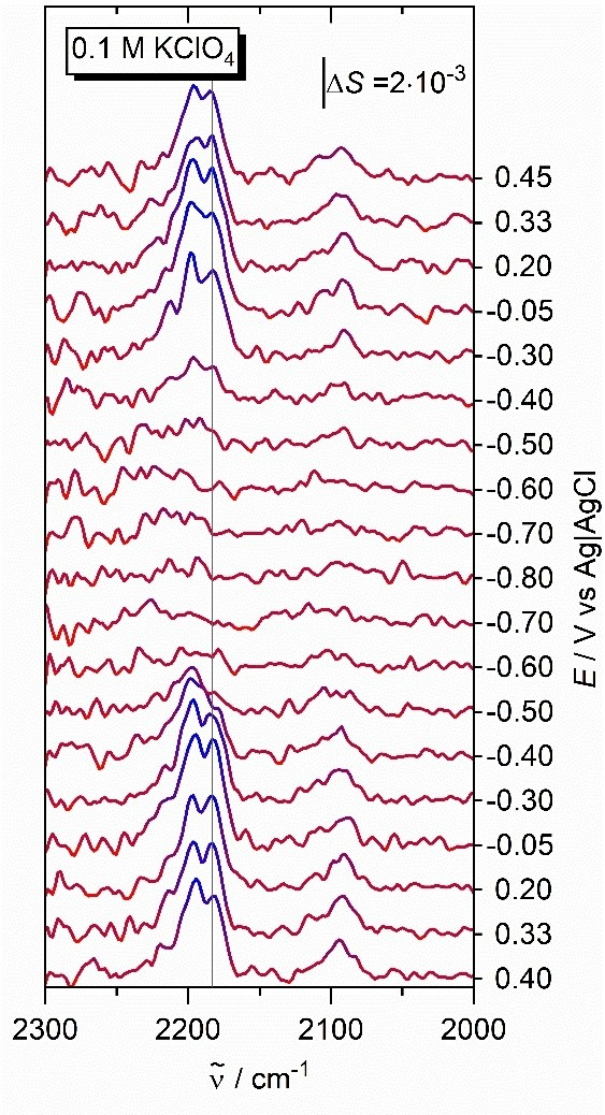

Figure 2. In situ PM IRRA spectra of the [C18C1Im-d_{37}][X] LB monolayer on the Au(111) surface in 0.1 M $KClO_4$ in H_2O solution in the 2300–2000 cm^{-1} spectral region at potentials marked in the figure. A thin solid line shows the position of the new IR absorption band.

potential scans in the potential range $0.40 < E < -0.40$ V versus Ag | AgCl (all potentials are referred versus Ag | AgCl reference electrode). In the spectral region of the $\nu_{as}(CD_2)$ mode, two strong peaks centered at 2197 (fwhm = 17 cm^{-1}) and 2182 cm^{-1} (fwhm = 15 cm^{-1}) were clearly seen in the PM IRRA spectra (Figures 2 and S1, Supporting Information). The $\nu_s(CD_2)$ mode appeared at 2091 cm^{-1}, and its fwhm equaled 15 cm^{-1}. The methylene-d_2 stretching modes in the monolayer films were broader than in the bulk phase, indicating an enhanced chain mobility in the adsorbed state.

At $E \leq -0.5$ V, the intensities of all IR absorption modes decreased and could not be distinguished from the background spectrum. A parallel decrease in the intensities of all three IR absorption modes was observed.

Next, the effect of the electrolyte composition, and thus of the counterion, on the spectroelectrochemical characterization of the IL monolayer was investigated. Figure 3 shows in situ PM IRRA spectra of the [C18C1Im-d_{37}][X] monolayer in a 0.1 M KCl solution. Interestingly, in 0.1 M KCl solution, the IL monolayer responded differently to electric potentials. In both negative and positive going potential scans, at $E > 0.33$ V and $E < -0.6$ V, the $\nu_{as}(CD_2)$ was centered at 2197 cm^{-1} and its fwhm equaled 18 cm^{-1} (Figure S1, Supporting Information). At $0.2 < E < -0.5$ V, next to the $\nu_{as}(CD_2)$ mode at 2197 cm^{-1} (fwhm = 15 cm^{-1}), a second absorption band at 2183 cm^{-1} (fwhm = 17 cm^{-1}) was present in the PM IRRA spectra. In all spectra shown in Figure 3, the $\nu_s(CD_2)$ mode was centered at 2093 cm^{-1}. In the KCl electrolyte solution, similar to the $KClO_4$ solution, the fluid perdeuterated alkyl chains have increased mobility. The intensity of the mode at 2183 cm^{-1} was very sensitive to the

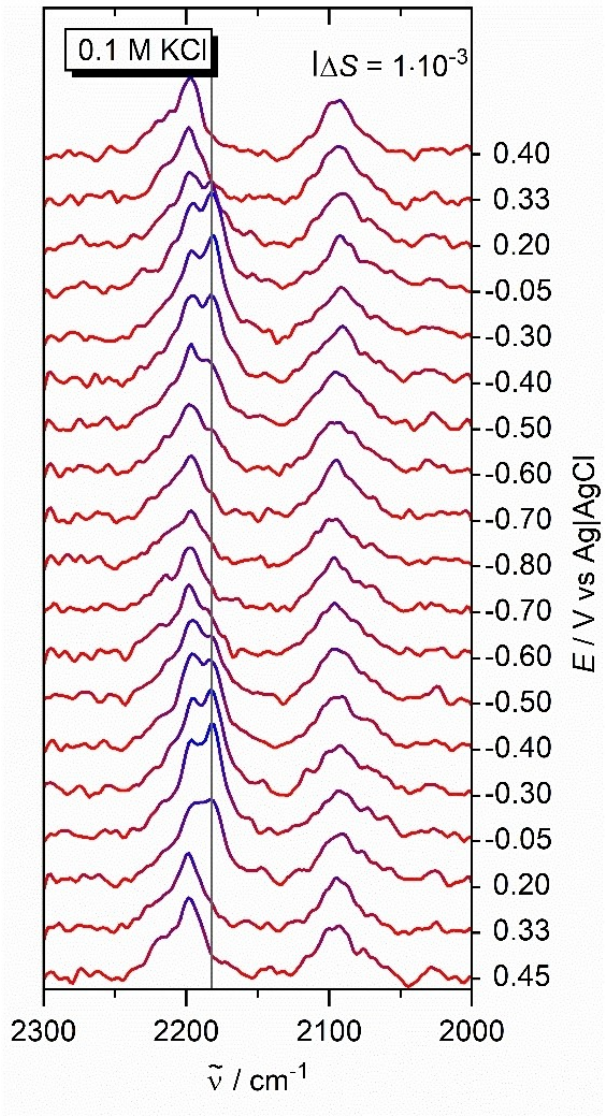

Figure 3. In situ PM IRRA spectra of the [C18C1Im-d_{37}][X] LB monolayer on the Au(111) surface in 0.1 M KCl in H_2O solution in the 2300–2000 cm^{-1} spectral region at potentials marked in the figure. A thin solid line shows the position of the new IR absorption band.

potential applied to the Au(111) electrode. In the potential range $0.05 < E < -0.3$ V, it became more intense than the $\nu_{as}(CD_2)$ mode at 2197 cm^{-1}. In contrast to the $KClO_4$ electrolyte solution, the intensities of $\nu_{as}(CD_2)$ and $\nu_s(CD_2)$ modes did not decrease to zero during the potential scan (Figure 3). However, their intensities changed as a function of the electrode potential and were stronger at positive- than at negative potentials.

To illustrate potential-driven spectral changes in the [C18C1Im-d_{37}][X] IL monolayer, difference spectra were calculated and are shown in S4 (Figures S4, S5, Supporting Information). Integral intensities of CD_2 stretching modes reflect the average orientation of the methylene groups in the alkyl chain.[9a,11a] In the [C18C1Im-d_{37}][X] monolayer, despite differences in the dynamics of potential-driven changes of the intensities of the methylene-d_2 stretching modes, similarities between both experiments were observed. First of all, the spectral changes shown in Figures 2 and 3 were reversible as a function of the electrode potential. Moreover, the positions of the absorption maxima of the $\nu_{as}(CD_2)$ and $\nu_s(CD_2)$ modes were independent of the electrode potential and corresponded to the liquid state of a perdeuterated chain.[12a,16b,20] This shows that the physical state of the alkyl chain (conformation) did not change during the potential scan. Increase in the number of gauche conformations in the alkyl chain leads to a hyposchromic shift of the methylene stretching modes, as for example observed in ionic liquids-water mixtures.[11b]

Except for the physical state (chain conformation), the position of the absorption maximum of the methylene groups depends on their substituents and thus on their location in a perdeuterated chain.[12] The frequencies of the CH stretching modes may be affected by the environment (polar, nonpolar) of the sample. To find the effect of the incorporation of the octadecyl-d_{37} chain in the polar (water) and nonpolar (heptane) environment on the IR spectra of the per-deuterated alkyl chains, quantum chemical calculations on the [C18C1Im-d_{37}][ClO_4] complex (ion pair) were performed.

Quantum chemical calculations of the [C18C1Im-d_{37}][ClO_4] ion pair

Prior to the calculation of harmonic frequencies, the structure of the [C18C1Im-d_{37}][ClO_4] complex (ion pair) was optimized (Figure 4).

For one ion pair, a large variety of conformations may be adopted. A model complex was constructed under the conditions listed below. In a hydrocarbon chain existing in a liquid state, the content of gauche units is close to 30%.[21] Thermotropic studies of the melting process of hydrocarbon chains in lipid molecules show that the gauche conformations appear more often at both terminals and are less probable in the central part of a hydrocarbon chain.[22] Thus, the quantum chemical calculations of the IR absorption modes were carried out for the octadecyl-d_{37} chain containing four gauche conformations (C2, C3, C15 and C17 in Figure 4). Hydrogen bonds originating from the H atoms of the imidazolium ring and its cationic charge lead to the association of anions either in the ring plane or above it. As the film is quite densely packed, we assumed that the ClO_4^- anion was positioned above the ring moiety.[11a,23]

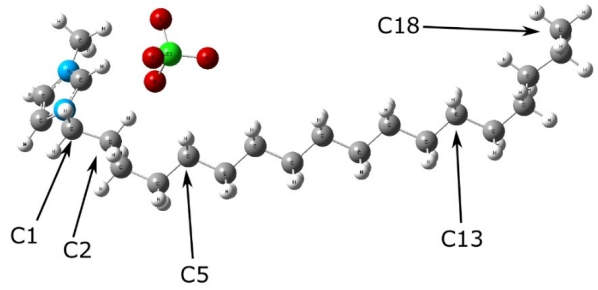

Figure 4. Optimized structure of the [C18C1Im-d_{37}][ClO_4] ion pair (PBE0-D3BJ/def2-TZVP). Only the C atoms on the perdeuterated alkyl chain are numbered due to their contribution the frequencies given in Tables S4–S6.

To simulate the chemical environment of the IL, an implicit solvation model was adopted. Cartesian coordinates of the optimized [C18C1Im-d_{37}][ClO_4] complex in vacuum, heptane (nonpolar environment), and water (polar environment) are listed in Tables S1–S3 (S5, Supporting Information). Vibrations of the methyl-d_3 and methylene-d_2 stretching modes were calculated for the [C18C1Im-d_{37}][ClO_4] IL ion pair in the different environments. In S5, Tables S4–S6, the wavenumbers of the methyl-d_3 and methylene-d_2 stretching modes are listed. Figure 5 shows the calculated IR spectra of the [C18C1Im-d_{37}][ClO_4] complex in water, heptane, and vacuum for the fwhm set to

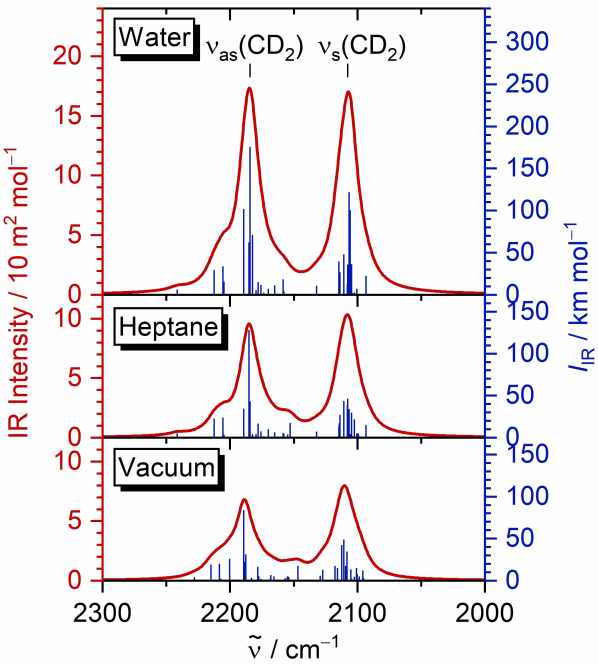

Figure 5. Calculated IR spectra of the [C18C1Im-d_{37}][ClO_4] monomer in water, in heptane, and in vacuum (PBE0-D3BJ/def2-TZVP); The full width at half maximum of the CD_2 stretching modes were set to 15 cm^{-1}. The red curve depicts the sum function of all modes. Blue line spectra show the integral intensity of all modes in this region.

15 cm^{-1}. Due to the scaling factor of 0.9575,[24] the absolute values of the vibrations matched the experimental values reasonably well. As listed in Tables S4–S6, the wavenumbers of the $\nu_{as}(CD_2)$ and $\nu_s(CD_2)$ modes depend on the position of the methylene-d_2 group in the chain. Note that only C atoms in the alkyl chain of the $[C18C1Im\text{-}d_{37}]^+$ cation are numbered (Figure 4). The CD_2 stretching modes at the C1 and C2 atoms appear at the highest wavenumbers, giving the $\nu_s(CD_2)$ mode around 2160–2150 cm^{-1} (Figure 5).

The corresponding $\nu_{as}(CD_2)$ modes overlay the $\nu_{as}(CD_3)$ mode. Similarly, for selectively perdeuterated acyl chain in phospholipids, a hypsochromic shift of fundamental methylene stretching modes located next to an electron-withdrawing moiety was observed. The $\nu_s(CD_2)$ mode at C2 and C3 atoms appeared at 2145–2137 cm^{-1}, while the corresponding $\nu_{as}(CD_2)$ mode was too weak and broad to measure.[12]

Independently of the environment of the alkyl chain in the $[C18C1Im\text{-}d_{37}][ClO_4]$ ion pair, the wavenumbers of the CD_2 stretching modes moved to lower wavenumbers, reaching a minimum for methylene groups present in the middle of the alkyl chain when the position of the methylene-d_2 group moved away from the head-group region. An increase in the frequency of the $C(2)D_2$ stretching modes was caused by the electrostatic charge distribution of the $[C18C1Im\text{-}d_{37}][ClO_4]$ complex, leading to an increase in the force constant. Despite the fact that the calculated wavenumbers of individual $\nu_{as}(CD_2)$ modes differ by up to 90 cm^{-1}, and of the $\nu_s(CD_2)$ modes by 60 cm^{-1} (S5, Supporting Information), the calculated spectra showed one well-defined absorption band each for the $\nu_{as}(CD_2)$ and $\nu_s(CD_2)$ mode (Figure 5). The experimental ATR IR spectrum also showed two methylene-d_2 stretching bands. Thus, a splitting of the CD_2 stretching modes in the $[C18C1Im\text{-}d_{37}][X]$ monolayer due to the differences in absorption frequencies of individual methylene groups was excluded. The intensity-weighted average position of the $\nu_{as}(CD_2)$ mode in the $[C18C1Im\text{-}d_{37}]^+$ cation in water, is 2188 cm^{-1}, while in heptane 2190 cm^{-1}, and in vacuum 2190 cm^{-1}. The weighted average wavenumber of the $\nu_s(CD_2)$ mode in water was 2110 cm^{-1}, in heptane 2112 cm^{-1}, and in vacuum 2112 cm^{-1}. In fact, the $\nu_{as}(CD_2)$ mode experiences a few cm^{-1} bathochromic shift in water, compared to heptane. The CH (CD) modes are not the most sensitive to the solvent effects; a dependence of the ν(CD) stretching mode on the solvent polarity and density has, however, been previously observed.[25] The ion pair used in the calculation, does not represent the monolayer on the Au(111) surface, however our results show a clear indication that the environment of the alkyl chain affects the position of the CD_2 stretching modes. Based on the results described above, we conclude that the new mode at 2182–2183 cm^{-1}, observed in the IL monolayers, originates from the $\nu_{as}(CD_2)$ mode in alkyl chains exposed to polar environment. The $\nu_{as}(CD_2)$ mode around 2195 cm^{-1} arises from the alkyl chains embedded in the nonpolar environment. Interestingly, no splitting of the $\nu_s(CD_2)$ mode was observed. Note that the experimental fwhm of this mode in the monolayer film is significantly larger than for a pure substance as well as for amphiphilic molecules containing perdeuterated alkyl chains aggregated into bilayers, in which the hydrocarbon chains face each other ensuring a nonpolar environment in this region.[12a,16b]

One may ask why the splitting of the methylene-d_2 stretching mode was observable in perdeuterated, but not in hydrogenated chains. The $\nu_{as}(CH_2)$ IR absorption mode is overlapped by two FR modes around 2940 and 2900 cm^{-1}.[26] Thus, the second component of the $\nu_{as}(CH_2)$ mode may overlap with one of the FR modes. In our previous studies, we observed an electric potential-dependent increase in the intensity around 2905 cm^{-1}, which, next to a FR, may contain a contribution from the $\nu_{as}(CH_2)$ mode.[11a] In contrast to the CH stretching-modes region, in the 2200–2000 cm^{-1} spectral region, the overtones and combinational modes do not overlap with the $\nu_{as}(CD_2)$ mode. They usually appear as separate, weak absorption bands.[16c,18,27] The separation between the $\nu_{as}(CD_2)$ and $\nu_s(CD_2)$ modes is close to 100 cm^{-1}, whereas between the $\nu_{as}(CH_2)$ and $\nu_s(CH_2)$ modes it is only 65–70 cm^{-1}. Due to a larger partition between $\nu_{as}(CD_2)$ and $\nu_s(CD_2)$ modes, a better separation of new IR absorption modes appearing in this spectral region is expected.

Molecular scale picture of potential-driven changes in the $[C18C1Im\text{-}d_{37}][X]$ ionic liquid monolayer

Having assigned the new IR absorption mode, we now discuss the origin of the splitting of the $\nu_{as}(CD_2)$ mode in IL monolayer films. The appearance of two $\nu_{as}(CD_2)$ modes depends on the potential applied to the Au(111) electrode, and on the chemical nature of the anion present in the electrolyte solution.

Our previous studies showed that in the monolayer films, the imidazolium ring adopts a well-defined, potential-independent, tilted toward Au(111) surface orientation, whereas the hydrocarbon chain responds to electric potentials.[11a] In addition to our own results, unusual assemblies of nonpolar fragments of ILs at electrified interfaces have recently been observed experimentally[2a,6c,29] and predicted in molecular dynamics calculations.[2a,b,7b]

In a 0.1 M $KClO_4$ solution, at potentials close to the potential zero charge of the Au(111) electrode ($E_{pzc} \approx 0.3$ V versus Ag|AgCl), the perchlorate anions were present in a monolayer, in the vicinity of the imidazolium ring, as illustrated in Figure 6(a) ($E = 0.45$ V and $E = 0.05$ V).[11a] Perchlorate ions have a chaotropic character and are weakly hydrated. Chaotropic anions have an affinity to neutral organic and inorganic compounds, such as lipid bilayers, membranes, polymers, or macrocyclic compounds.[30] The methylene-d_2 groups in the alkyl chains in the $[C18C1Im\text{-}d_{37}]^+$ cations embedded in a polar microenvironment produce the $\nu_{as}(CD_2)$ mode at 2182–2183 cm^{-1}. Other methylene groups are embedded in the hydrophobic environment of the alkyl chains and produce the $\nu_{as}(CD_2)$ mode at 2195–2197 cm^{-1}.

In addition, a potential driven change in the Au(111) surface may be a driving force for adsorption/desorption of ions and their particular orientation on the metal surface.[28] The effect of the surface reconstruction cannot be elucidated from our measurements. However, when a densely packed monolayer

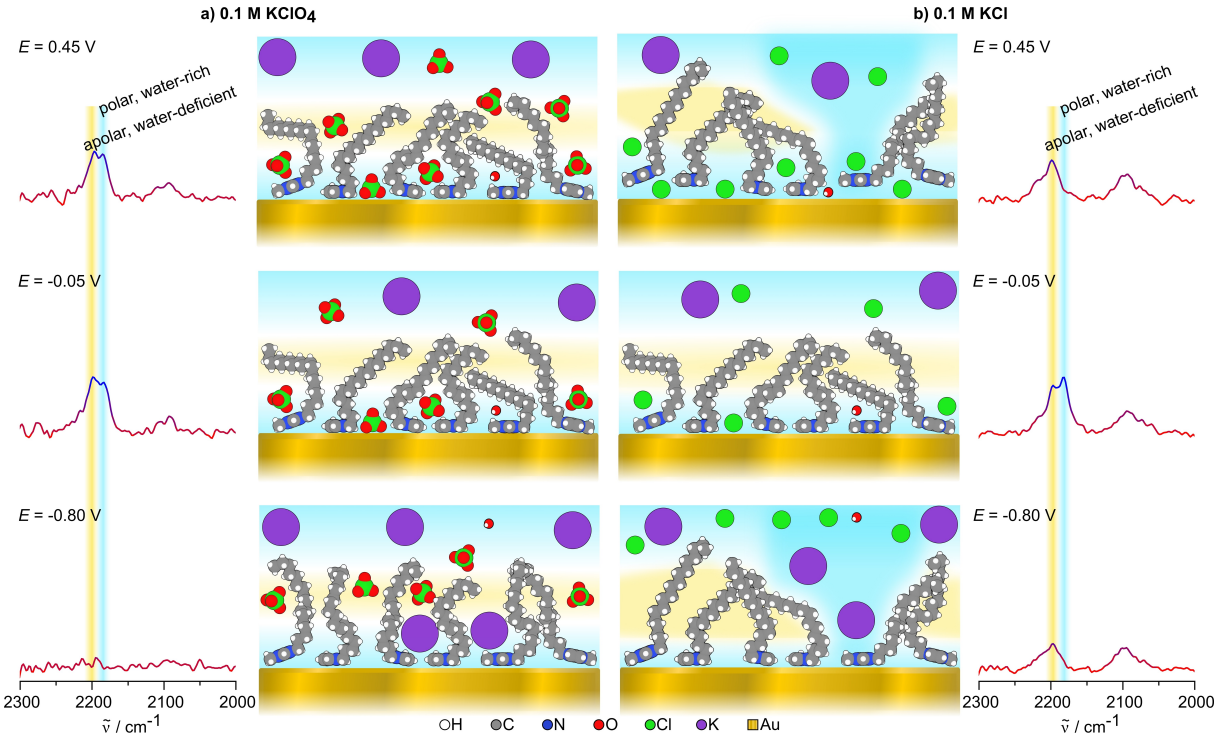

Figure 6. Illustration of the molecular scale order and segregation between polar and nonpolar microenvironments in the [C18C1Im-d_{37}][X] IL monolayer on the Au(111) surface in a) $KClO_4$ and b) KCl electrolyte solutions.

film is used, changes in the surface will not profoundly affect its structure. Differences in the microenvironment within the [C18C1Im-d_{37}][X] monolayer lead to a segregation between the polar and nonpolar environment in the IL film (Figure 6a, $E=$ 0.45 V and $E=0.05$ V). A negative potential shift (Figure 6a, $E=-0.8$ V) lead to an electrostatic repulsion of the perchlorate anions from the vicinity of the Au(111) electrode, as demonstrated the electrochemical results.[11a] Simultaneously, the intensities of the methylene stretching mode decreased, indicating a preferential up-ward orientation of the perdeuterated chains (Figure 6a, $E=-0.8$ V). A potential-driven movement of the anions from the Au surface through the monolayer into the solution phase is connected with a reorientation of the alkyl chains.

Chloride ions have a more kosmotropic character and exhibit a significantly lower ability than the perchlorate ions to penetrate into the hydrophobic region of the monolayer. In contrast, they interact with H atoms in the imidazolium ring and are preferably found in the plane of the ring. However, their location above the ring cannot be excluded.[23,31] XPS results (Figure S6, Supporting Information) indicate that the chloride ions are adsorbed directly onto the Au surface, as well as being incorporated onto the monolayer, making direct contact with the imidazolium ring.[14] Above the potential of zero charge, chloride ions adsorb specifically onto the Au(111) surface. Thus, the chloride ions are attracted to the electrode surface and leave the monolayer. The alkyl chains gain a nonpolar environment which is consistent with the presence of only one $\nu_{as}(CD_2)$ mode at 2197 cm^{-1} as illustrated in Figure 6b ($E=0.45$ V). A moderately negative potential shift weakens the binding of chloride ions to the Au surface and brings a local hydrophilic environment into the vicinity of the imidazolium ring. In consequence these chain fragments give rise to the $\nu_{as}(CD_2)$ mode at 2183 cm^{-1} (Figure 6b, $E=-0.05$ V). This situation is similar for both anions. In the monolayer fragments, that are poor in chloride anions, the van der Waals interactions between the perdeuterated chains ensure a nonpolar microenvironment in the chain region, producing the $\nu_{as}(CD_2)$ mode at 2197 cm^{-1}. A further negative potential shift leads to the desorption and removal of the hydrophilic, kosmotropic chloride ions from the monolayer. One $\nu_{as}(CD_2)$ mode, characteristic for the nonpolar environment in the monolayer, is seen in the PM IRRA spectra (Figure 6b, $E=-0.8$ V). The intensity of the $\nu_{as}(CD_2)$ did not decrease to zero, as it was observed in the $KClO_4$ electrolyte solution. It indicates that the alkyl chains changed little their orientation. Since the kosmotropic ions do not penetrate into a hydrocarbon chain region, no significant alignment of the chain region was necessary.

Segregation between the polar and nonpolar microenvironments in the alkyl chain fragment of the IL monolayer depends on the electrode potential and on the character of the anion present in the electrolyte solution and possibly on the potential-driven reorientation of the substrate surface. Thus, the electrode closest electrical double layer structure and hydrophilicity/hydrophobicity of ILs in water may be tuned by the selection of either chaotropic or kosmotropic anions.

Conclusion

Our results demonstrate interesting dynamics of electric potential-driven changes in the [C18C1Im-d_{37}][X] IL monolayers on the Au(111) electrode surface. The imidazolium ring had a rather stable, potential-independent orientation[11a] whereas the alkyl chain in the cation respond to electric potentials. At positive potentials the anions accumulate in the vicinity of the imidazolium ring, producing locally a hydrophilic environment into the chain region while other parts of the chains have nonpolar surroundings. A negative potential shift strengthened the attraction of imidazolium cations toward the Au(111) surface and, as pointed by electrochemical measurements,[11a] led to a movement of anions through the [C18C1Im-d_{37}][X] monolayer.

Second, we demonstrated the great advantage of IR spectroscopy for in situ studies of microheterogeneity in ILs. IRS is sensitive not only to the composition and conformation of organic molecules, but also to the environment of the sample. The alkyl chain region of the [C18C1Im-d_{37}][X] monolayer experienced a potential-dependent separation between a polar and nonpolar environment. Despite the fact that the frequencies of the IR absorption modes of the CD_2 (CH_2) groups did not respond strongly to solvents with different polarities, a bathochromic shift of these modes in polar solvents was expected[25] and indeed predicted by quantum chemical calculations. Differences between the polar and nonpolar microenvironment in the monolayer are exhibited as a splitting of the CD_2 asymmetric stretching mode. Electric potentials and nature of the counterion change the balance between these two microenvironments. The high wavenumber component of the ν_{as} (CD_2) mode, centered at 2195–2197 cm^{-1}, corresponds to the hydrophobic microenvironment in the alkyl chain region of the IL. The low wavenumber $\nu_{as}(CD_2)$ mode, centered at 2182–2183 cm^{-1}, reflects a polar microenvironment introduced by the anions and water molecules into the chain region of the [C18C1Im-d_{37}][X] monolayer.

The spectral isolation of CD stretching modes from other fundamental modes allowed for in-depth analysis of the environmental effects on the position and number methylene-d_2 stretching modes. Quantum chemical calculations of the IR spectra of the studied IL support the experimental results. The applicability of quantum chemical calculations for computation of the IR absorption modes of organic molecules is another great advantage of the IRS experiments, since it allows for the verification and assignment of IR absorption modes, facilitating the analysis of experimental results.

The synthesis pathway of perdeuterated ILs proposed here involves only two steps. The simplicity of the synthesis ensures an economic way of obtaining large amounts of isotopically substituted ILs and is thus beneficial for in situ spectroscopic studies of their properties. This work clearly demonstrates the advantage of the use of ILs with perdeuterated alkyl chains, which results in better-resolved IR spectra when compared to their hydrogenated analogues. In other words, we were able to follow the dynamics of electric potential dependent local changes in the environment in interfacial assemblies of ILs.

Finally, a selective isotopic substitution of IL present in the layers closest to the electrode surface makes it possible to distinguish surface from solution species. These studies are in progress. Use of perdeuterated ILs has the potential to answer fundamental questions about their electrochemical characteristics.

Experimental Section

Chemicals

The following high-purity components were purchased and used without further purification: argon (5 N, Air Liquide, Düsseldorf, Germany), chloroform (Sigma-Aldrich, Steinheim, Germany), ethanol (Sigma-Aldrich, Steinheim, Germany), hydrogen peroxide (30%, Sigma-Aldrich, Steinheim, Germany), n-octadecanol-d_{37} (Cambridge Isotope Laboratories, Andover, USA), potassium chloride (Roth, Karlsruhe, Germany), potassium perchlorate (Acros Organics, Geel, Belgium). Deionized water was obtained from a PureLab Classic system (Elga LabWater, Celle, Germany, resistivity $\geq$ 18.2 MΩ cm).

Synthesis of 1-methyl-3-(octadecyl-d_{37})imidazolium trifluoromethanesulfonate

A solution of octadecyl-d_{37} triflate (150 mg, 0.341 mmol, 1.0 equiv.) and methylimidazole (38 mg, 0.463 mmol, 1.4 equiv.) in acetone (1 mL) was stirred in a tightly closed reaction tube for 22.5 h at 130 °C. After evaporation of the volatiles, the residue was recrystallized from MTBE (50 mL) to furnish the product (129 mg, 0.247 mmol, 72%) as colorless solid, mp. 66 °C. ^{1}H NMR (300 MHz, acetone-d_6): $\delta = 4.05$ (s, 3H), 7.69–7.81 (m, 2H), 9.11 (s, 1H) ppm. ^{13}C{^{1}H} NMR (75 MHz, acetone-d_6): $\delta = 36.68$ (CH_3), 123.43 (CH), 124.82 (CH), 137.70 (CH) ppm. IR (ATR): $\lambda^{-1} = 3153$ (w), 3105 (w), 2194 (m), 2090 (m), 1563 (w), 1255 (s), 1226 (m), 1160 (s), 1091 (m), 1031 (s), 846 (w), 757 (m), 639 (s) cm^{-1}. HR-MS (ESI, pos. mod.): calcd. 372.5746 (for $C_{22}H_6D_{37}N_2^+$), found 372.5750 [M^+-OTf]. $C_{23}H_6D_{37}F_3N_2O_3S$ (521.89).

Langmuir-Blodgett transfer

Surface pressure versus mean molecular area isotherms were recorded using a KSV LB Mini Trough (KSV Ltd., Helsinki, Finland) equipped with two hydrophilic barriers and a Wilhelmy balance with a paper Wilhelmy plate. Prior to use, it was cleaned with copious amounts of water, ethanol, wiped with chloroform, and rinsed with ethanol and water again. After each rinse, the surface was dried with delicate task wipes (Kimtech). Fresh solutions of [C18C1Im-d_{37}][TfO] in chloroform (0.8 mg mL^{-1}) were prepared daily. For the isotopic dilution experiment of [C18C1Im-h_{43}][Cl]:[C18C1Im-d_{37}][TfO] = 1:10 molar ratio, a solution of 12.8 mg [C18C1Im-h_{43}][Cl] + 1.8 mg [C18C1Im-d_{37}][TfO] in 20 mL $CHCl_3$ was prepared, yielding an averaged mass concentration of 0.73 g L^{-1}. Using a microsyringe (Hamilton, Reno, USA), a few microliters of the ILs' solution were placed either on the 0.1 M $KClO_4$ or 0.1 M KCl aqueous subphase and left 5 min for solvent evaporation. To protect the experimental setup from dust, it was placed in a laminar flow hood. IL monolayers were compressed to a surface pressure of 25 mN m^{-1} and transferred by LB vertical withdrawing of the Au(111) disc electrode (12 mm diameter, polished with an orientation accuracy $< 1°$, MaTeck, Germany) with a speed of 20 mm s^{-1}. After transfer, the gold substrate was dried overnight in argon atmosphere.

PM IRRAS

PM IRRA spectra were measured with a Vertex 70 spectrometer and an external reflection setup (Bruker, Ettlingen, Germany) containing a photoelastic modulator with the frequency of 50 kHz and a demodulator PMA 50 (Hinds Instruments, Hillsboro, OR, USA).

PM IRRA spectra were recorded at the Au(111)|air interface at the angle of incidence of the IR light 80° versus surface normal. In all experiments the half-wave retardation was set to 2200 cm^{-1} and the spectrometer resolution to 4 cm^{-1}. The PM IRRA spectra of the [C18C1Im-d_{37}][X] monolayer transferred from the 0.1 M $KClO_4$ subphase onto the Au(111) electrode surface were recorded several times over first 20 h after the film transfer. Each spectrum contained 512 co-added spectra. These spectra were averaged, as no changes were observed.

In situ PM IRRA spectra were recorded in a three-electrode spectroelectrochemical cell at various potentials applied to the Au(111) electrode, which simultaneously served as a mirror for the IR light. All glass and Teflon ware were cleaned with copious amounts of water, ethanol, water, and dried overnight in an oven. A CaF_2 equilateral prism (Bioxin Photoelectric Co. Ltd., Changchun, China) was used as an optical window for the IR radiation. Before assembly of the spectroelectrochemical cell, the prism was washed with water and ethanol and cleaned for 10 min in the UV/ozone chamber. The spectroelectrochemical cell has a built-in platinum counter electrode. The reference electrode was Ag|AgCl in sat. KCl in H_2O. The cell was filled with 0.1 M $KClO_4$ or 0.1 M KCl as the electrolyte in H_2O and purged with argon for 1 h to remove oxygen. The potential was stepped and hold for 20 s before starting the collection of 500 spectral scans. In each experiment, four to five negatively going and positively going potential scans were recorded. Each potential scan was analyzed separately. Single spectra shown in this article correspond to an average of 2000 or 2500 scans recorded for 0.1 M $KClO_4$ and 0.1 M KCl electrolytes, respectively. The angle of incidence of the IR light was set to 54° with respect to the surface normal. PM IRRA spectra were processed using OPUS v5.5 software (Bruker, Ettlingen, Germany). Spectra depicted in this manuscript show the differential reflectivity of the organic molecules present on the metal surface after background subtraction by spline-interpolation as a function of wavenumbers, as explained in S2.

ATR IRS

Attenuated total reflection infrared spectroscopy (ATR IRS) spectra were recorded by co-adding 64 scans with a nominal resolution of 2 cm^{-1} of the pure [C18C1Im-d_{37}][TfO] powder on a single reflection silicon prism using a MVP-Pro ATR unit (Harrick Scientific Products, Inc., Pleasantville, NY, USA) and the Bruker Vertex 70 spectrometer.

Computational details

The electronic structure calculations were performed using the Gaussian16.a03 program package.[32] Throughout the calculations, density functional theory (DFT) on the PBE0[33a]/def2-TZVP[33b] level of theory in conjunction with Grimme's D3 dispersion correction[34a] with Becke-Johnson damping[34b] was employed. Geometry optimization lead to stationary points without imaginary frequencies. The harmonic frequencies were obtained after full structural optimization of the respective geometry and afterwards scaled by a factor of 0.9575.[24] For solvation, the Polarizable Continuum Model (PCM) with of water ($\varepsilon = 78.3553$) and heptane ($\varepsilon = 1.9113$) was applied.

Acknowledgements

I.B. acknowledges the financial support from the DFG project BR-3961-5. Calculations were performed at the HPC Cluster CARL, located at the University of Oldenburg and founded by DFG through the Major Research Instrumentation Program (INST 184/157.1 FUGG), and the Ministry of Science and Culture (MWK) of the State of Lower Saxony. English language services were provided by stels-ol.de. Open Access funding enabled and organized by Projekt DEAL.

Conflict of Interest

The authors declare no conflict of interest.

Keywords: ionic liquid · IR spectroscopy · LB monolayer · nanosegregation · perdeuterated hydrocarbon chain

[1] a) K. Dong, X. Liu, H. Dong, X. Zhang, S. Zhang, *Chem. Rev.* **2017**, *117*, 6636–6695; b) L. Xu, E. I. Izgorodina, M. L. Coote, *J. Am. Chem. Soc.* **2020**, *142*, 12826–12833; c) R. Hayes, G. G. Warr, R. Atkin, *Chem. Rev.* **2015**, *115*, 6357–6426; d) J. Luczak, C. Jungnickel, I. Lacka, S. Stolte, J. Hupka, *Green Chem.* **2010**, *12*, 593–601.

[2] a) X. Mao, P. Brown, C. Červinka, G. Hazell, H. Li, Y. Ren, D. Chen, R. Atkin, J. Eastoe, I. Grillo, A. A. H. Padua, M. F. Costa Gomes, T. A. Hatton, *Nat. Mater.* **2019**, *18*, 1350–1357; b) S. Katakura, N. Nishi, K. Kobayashi, K. Amano, T. Sakka, *J. Phys. Chem. C* **2020**, *124*, 7873–7883; c) E. J. M. Filipe, P. Morgado, M. Teixeira, K. Shimizu, N. Bonatout, M. Goldmann, J. N. Canongia Lopes, *Chem. Commun.* **2016**, *52*, 5585–5588.

[3] a) M. A. Gebbie, H. A. Dobbs, M. Valtiner, J. N. Israelachvili, *Proc. Natl. Acad. Sci. USA* **2015**, *112*, 7432–7437; b) Y. Wang, G. A. Voth, *J. Am. Chem. Soc.* **2005**, *127*, 12192–12193; c) R. Elfgen, O. Hollóczki, B. Kirchner, *Acc. Chem. Res.* **2017**, *50*, 2949–2957; d) R. Atkin, S. M. C. Bobillier, G. G. Warr, *J. Phys. Chem. B* **2010**, *114*, 1350–1360.

[4] a) R. S. Anaredy, S. K. Shaw, *Langmuir* **2016**, *32*, 5147–5154; b) R. S. Anaredy, S. K. Shaw, *J. Phys. Chem. C* **2019**, *123*, 8975–8982.

[5] a) S. Perkin, L. Crowhurst, H. Niedermeyer, T. Welton, A. M. Smith, N. N. Gosvamia, *Chem. Commun.* **2011**, *47*, 6572–6574; b) K. Ma, R. Jarosova, G. M. Swain, G. J. Blanchard, *Langmuir* **2016**, *32*, 9507–9512; c) Y. Wang, R. Jarošová, G. M. Swain, G. J. Blanchard, *Langmuir* **2020**, *36*, 3038–3045; d) T. Cremer, M. Stark, A. Deyko, H. P. Steinrück, F. Maier, *Langmuir* **2011**, *27*, 3662–3671; e) J. N. A. Canongia Lopes, A. A. H. Padua, *J. Phys. Chem. B* **2006**, *110*, 3330–3335.

[6] a) R. Atkin, S. Zein El Abedin, R. Hayes, L. H. S. Gasparotto, N. Borisenko, F. Endres, *J. Phys. Chem. C* **2009**, 13266–13272; b) M. V. Fedorov, A. A. Kornyshev, *Chem. Rev.* **2014**, *114*, 2978–3036; c) R. Wen, B. Rahn, O. M. Magnussen, *Angew. Chem. Int. Ed.* **2015**, *54*, 6062–6066; *Angew. Chem.* **2015**, *127*, 6160–6164; d) D. W. Bruce, C. P. Cabry, J. N. Canongia Lopes, M. L. Costen, L. D'Andrea, I. Grillo, B. C. Marshall, K. G. McKendrick, T. K. Minton, S. M. Purcell, S. Rogers, J. M. Slattery, K. Shimizu, E. Smoll, M. A. Tesa-Serrate, *J. Phys. Chem. B* **2017**, *121*, 6002–6020.

[7] a) T. Pajkossy, C. Müller, T. Jacob, *Phys. Chem. Chem. Phys.* **2018**, *20*, 21241–21250; b) J. Qin, M. Wang, Y. Wang, C. Wang, Y. Lu, F. Huo, H. He, *ChemElectroChem* **2021**, *8*, 2105-2112.

[8] R. Wen, B. Rahn, O. M. Magnussen, *J. Phys. Chem. C* **2016**, *120*, 15765–15771.

[9] a) I. Brand, *Application of polarization modulation infrared reflection absorption spectroscopy in electrochemistry*, Springer Nature, Cham, **2020**; b) A. H. Kycia, Z. F. Su, C. L. Brosseau, J. Lipkowski, in *Vibration spectroscopy at electrified interfaces* (Eds.: A. Wieckowski, C. Korzeniewski, B. Braunschweig), Wiley, Heidelberg, **2013**, pp. 345–417; c) J. Lipkowski, *J. Solid State Electrochem.* **2020**, *24*, 2121–2123.

[10] a) R. A. MacPhail, H. L. Strauss, R. G. Snyder, C. A. Elliger, *J. Phys. Chem.* **1984**, *88*, 334–341; b) R. G. Snyder, H. L. Strauss, C. A. Elliger, *J. Phys. Chem.* **1982**, *86*, 5145–5150.

[11] a) T. Sieling, I. Brand, *ChemElectroChem* **2020**, *7*, 3233–3243; b) Y. Jeon, J. Sung, D. Kim, C. Seo, H. Cheong, Y. Ouchi, R. Ozawa, H. Hamaguchi, *J. Phys. Chem. B* **2008**, *112*, 923–928.
[12] a) D. G. Cameron, H. L. Casal, H. H. Mantsch, Y. Boulanger, I. C. P. Smith, *Biophys. J.* **1981**, *35*, 1–16; b) S. C. Hsi, A. P. Tulloch, H. H. Mantsch, D. G. Cameron, *Chem. Phys. Lipids* **1982**, *31*, 97–103.
[13] K. Fujii, R. Kanzaki, T. Takamuku, Y. Kameda, S. Kohara, M. Kanakubo, M. Shibayama, S. Ishiguro, Y. Umebayashi, *J. Chem. Phys.* **2011**, *135*, 244502 244501–244512.
[14] T. Sieling, J. Christoffers, I. Brand, *ACS Sustainable Chem. Eng.* **2019**, *7*, 11593–11602.
[15] T. Alpers, M. Schmidtmann, T. W. T. Muesmann, O. Temme, J. Christoffers, *Eur. J. Org. Chem.* **2017**, 4283–4290.
[16] a) S. Sunder, D. G. Cameron, H. L. Casal, Y. Boulanger, H. H. Mantsch, *Chem. Phys. Lipids* **1981**, *28*, 137–148; b) A. R. Dluhy, R. Mendelsohn, H. L. Casal, H. H. Mantsch, *Biochemistry* **1983**, *22*, 1170–1171; c) M. Masat, Z. Sofer, J. Michl, *Langmuir* **2017**, *17*, 5613–5616; d) E. Tyrode, J. Heldberg, *J. Phys. Chem. C* **2016**, *2012*, 1080–1091.
[17] M. V. Fraile, B. Patron-Gallardo, L. Lopez-Rodriguez, P. Carmona, *Chem. Phys. Lipids* **1999**, *97*, 119–128.
[18] M. R. Bunow, I. W. Levin, *Biochim. Biophys. Acta* **1977**, *489*, 191–206.
[19] R. Mendelsohn, T. Taraschi, *Biochemistry* **1978**, *17*, 3944–3949.
[20] C. L. Brosseau, J. Leitch, X. Bin, M. Chen, S. G. Roscoe, J. Lipkowski, *Langmuir* **2008**, *24*, 13058–13067.
[21] S. A. Kirsch, R. A. Böckmann, *Biophys. J.* **2019**, *116*, 2131–2148.
[22] a) A. Seelig, J. Seelig, *Biochemistry* **1974**, *13*, 4839–4845; b) P. L. Yeagle, in *The membranes of cells*, Academic Press, New York, **2016**, 155–188.
[23] F. Dommert, J. Schmidt, C. Krekeler, Y. Y. Zhao, R. Berger, L. Delle Site, C. Holm, *J. Mol. Liq.* **2010**, *152*, 2–8.
[24] M. K. Kesharwani, B. Brauer, J. M. L. Martin, *J. Phys. Chem. A* **2015**, *119*, 1701–1714.
[25] R. A. Nyquist, *Appl. Spectrosc.* **1993**, *47*, 560–565.
[26] a) P. T. T. Wong, H. H. Mantsch, *Chem. Phys. Lipids* **1988**, *46*, 213–224; b) S. Abbate, G. Zerbi, S. L. Wunder, *J. Phys. Chem.* **1982**, *86*, 3140–3149.
[27] S. Sunder, D. Cameron, H. H. Mantsch, H. J. Bernstein, *Can. J. Chem.* **1978**, *56*, 2121–2126.
[28] a) U. E. Zhumaev, I. V. Pobelov, A. V. Rudnev, A. Kuzume, T. Wandlowski, *Electrochem. Commun.* **2014**, *44*, 31–33; b) W. Gao, T. A. Baker, L. Zhou, D. S. Pinnaduwage, E. Kaxiras, C. M. Friend, *J. Am. Chem. Soc.* **2008**, *130*, 3560–3565.
[29] B. Wu, J. P. Breen, X. Xing, M. D. Fayer, *J. Am. Chem. Soc.* **2020**, *142*, 9482–9492.
[30] a) K. I. Assaf, W. M. Nau, *Angew. Chem. Int. Ed.* **2018**, *57*, 13968–13981; *Angew. Chem.* **2018**, *130*, 14164–14177; b) R. Fernandez-Alvarez, V. Dordovic, M. Uchman, P. Matehicek, *Langmuir* **2018**, *34*, 3541–3554.
[31] H. Weingärtner, *Angew. Chem. Int. Ed.* **2008**, *47*, 654–670; *Angew. Chem.* **2008**, *120*, 664–682.
[32] M. J. Frisch, G. W. Trucks, H. B. Schlegel, G. E. Scuseria, M. A. Robb, J. R. Cheeseman, G. Scalmani, V. Barone, G. A. Petersson, H. Nakatsuji, X. Li, M. Caricato, A. V. Marenich, J. Bloino, B. G. Janesko, R. Gomperts, B. Mennucci, H. P. Hratchian, J. V. Ortiz, A. F. Izmaylov, J. L. Sonnenberg, D. Williams-Young, F. Ding, F. Lipparini, F. Egidi, J. Goings, B. Peng, A. Petrone, T. Henderson, D. Ranasinghe, V. G. Zakrzewski, J. Gao, N. Rega, G. Zheng, W. Liang, M. Hada, M. Ehara, K. Toyota, R. Fukuda, J. Hasegawa, M. Ishida, T. Nakajima, Y. Honda, O. Kitao, H. Nakai, T. Vreven, K. Throssell, J. J. A. Montgomery, J. E. Peralta, F. Ogliaro, M. J. Bearpark, J. J. Heyd, E. N. Brothers, K. N. Kudin, V. N. Staroverov, T. A. Keith, R. Kobayashi, J. Normand, K. Raghavachari, A. P. Rendell, J. C. Burant, S. S. Iyengar, J. Tomasi, M. Cossi, J. M. Millam, M. Klene, C. Adamo, R. Cammi, J. W. Ochterski, R. L. Martin, K. Morokuma, O. Farkas, J. B. Foresman, D. J. Fox, *Gaussian 16*, Revision A.03 ed., Gaussian, Inc., Wallingford, CT, USA, **2016**.
[33] a) C. B. V. Adamo, *J. Chem. Phys.* **1999**, *110*, 6158–6170; b) F. Weigend, R. Ahlrichs, *Phys. Chem. Chem. Phys.* **2005**, *7*, 3297–3305.
[34] a) S. Grimme, J. Antony, S. Ehrlich, H. Krieg, *J. Chem. Phys.* **2010**, *132*, 154104–154101 - 154104–154119; b) S. Grimme, S. Ehrlich, L. Goerigk, *J. Comput. Chem.* **2011**, *32*, 1456–1465.

Manuscript received: June 30, 2021
Accepted manuscript online: September 12, 2021
Version of record online: November 12, 2021

